Open access • Journal Article • DOI:10.1016/J.COMPOSITESB.2014.01.023

Explicit solutions for the modeling of laminated composite plates with arbitrary stacking sequences — Source link

Philippe Vidal, Laurent Gallimard, Olivier Polit

Institutions: University of Paris

Published on: 01 Apr 2014 - Composites Part B-engineering (Elsevier)

Topics: Displacement field and Finite element method

Explicit solutions for the modeling of laminated composite plates with arbitrary stacking sequences

Philippe Vidal, L. Gallimard, O. Polit

Explicit solutions for the modeling of laminated composite plates with arbitrary stacking sequences

P. Vidal *, L. Gallimard, O. Polit

Laboratoire Energétique, Mécanique, Electromagnétisme – EA4416, Université Paris Ouest Nanterre-La Défense, 50 rue de Sèvres, 92410 Ville d'Avray, France

A B S T R A C T

In this paper, a method to compute explicit solutions for laminated plate with arbitrary stacking sequences is presented. This technique is based on the construction of an a posteriori Reduced-Order Model using the so-called Proper Generalized Decomposition. The displacement field is approximated as a sum of separated functions of the in-plane coordinates x, y, the transverse coordinate z and the orientation of each ply θ_i. This choice yields to an iterative process that consists of solving a 2D and some 1D problems successively at each iteration. In the thickness direction, a fourth-order expansion in each layer is considered. For the in-plane description, classical Finite Element method is used. The functions of θ_i are discretized with linear interpolations. Mechanical tests with different numbers of layers are performed to show the accuracy of the method.

1. Introduction

Composite and sandwich structures are widely used in the industrial field due to their excellent mechanical properties, especially their high specific stiffness and strength. In this context, they can be subjected to severe mechanical loads. For laminated composite design, accurate knowledge of displacements and stresses is required. Moreover, the choice of the stacking sequences has an important influence on the behavior of the structures. The classical way consists in performing different computations with a fixed value of each orientation of the plies. The present approach based on the Proper Generalized Decomposition (PGD) aims at building the explicit solutions with respect to any stacking sequences avoiding the computational cost of numerous computations.

According to published research, various theories in mechanics for the modeling of composite structures have been developed. On the one hand, the Equivalent Single Layer approach (ESL) in which the number of unknowns is independent of the number of layers, is used. But, the transverse shear and normal stresses continuity on the interfaces between layers are often violated. We can distinguish the classical laminate theory [1] (unsuitable for composites and moderately thick plates), the first order shear deformation theory [2], and higher order theories with displacement [3–10] and mixed [11,12] approaches. On the other hand, the Layerwise approach (LW) aims at overcoming the restriction of the ESL concerning the discontinuity of out-of-plane stresses on the interface layers and taking into account the specificity of layered structure. But, the number of degrees of freedom (dofs) depends on the number of layers. We can mention the folllowing contributions [13–17] within a displacement based approach and [18,11,19] within a mixed formulation. As an alternative, refined models have been developed in order to improve the accuracy of ESL models avoiding the additional computational cost of LW approach. So, a family of models, denoted zig-zag models, was derived in [20–22] from the studies described in [23,24]. Note also the refined approach based on the Sinus model [25–27]. This above literature deals with only some aspects of the broad research activity about models for layered structures and corresponding finite element formulations. An extensive assessment of different approaches has been made in [28–32].

Over the past years, the so-called Proper Generalized Decomposition (PGD) [33] has shown interesting features in the reduction model framework. A separated representation of variables called radial approximation was also introduced in the context of the LATIN method [34] for reducing computational costs and used to solve parametric problems [35]. For the scope of our study, the PGD has been successfully applied for the modeling of composite beams and plates [36–38]. The principle of the method consists in using separated representation of the unknown fields to build an approximate solution of the partial differential equations. A first attempt to obtain analytical solutions for composite plate based on a Navier-type solution with a separation of variables can also be found in [39].

* Corresponding author. Tel.: +33 140974855.
E-mail address: philippe.vidal@u-paris10.fr (P. Vidal).

This work aims at modeling composite plate structures regardless of the stacking sequences. For this purpose, the present approach is based on the separation representation where the displacements are written under the form of a sum of products of (i) bidimensional polynomials of (x, y), (ii) unidimensional polynomials of z and (iii) unidimensional polynomials of the orientations of the plies θ_i. As in [38], a piecewise fourth-order Lagrange polynomial of z is chosen as it is particularly suitable to model composite structures. As far as the variation with respect to the in-plane coordinates is concerned, a 2D eight-node quadrilateral Finite Element (FE) is employed. The functions of the orientations of each ply are piecewise linear. Finally, the deduced non-linear problem implies the resolution of $NC+2$ linear problems alternatively (NC is the number of layers). This process yields to a 2D and 1D problems in which the number of unknowns is smaller than in a Layerwise approach. Finally, the solution depends explicitly on the fibers orientation of each ply.

We now outline the remainder of this article. First, the reference mechanical formulation is recalled. Then, the resolution of the parametrized problem by the PGD is described. The particular assumption on the displacements yields a non-linear problem which is solved by an iterative process. Then, the FE approximations are described. Finally, numerical tests are performed. A one-layer case is first considered to assess and illustrate the behavior of the method. The influence of the discretization of the functions depending on the orientation of the plies is shown. Two-layer and four-layer configurations are also addressed. The accuracy of the results is evaluated by comparison with reference solutions issued from PGD solutions with different fixed stacking sequences using the work developed in [38].

2. Reference problem description

2.1. The governing equations

Let us consider a plate occupying the domain $\mathcal{V} = \Omega \times \Omega_z$ bounded by $\partial\Omega$ with $\Omega_z = \left[-\frac{h}{2}, \frac{h}{2}\right]$ in a Cartesian coordinate system (x, y, z). The plate is defined by an arbitrary region Ω, in the (x, y) plane, located at the midplane $z = 0$, and by a constant thickness h. See Fig. 1.

2.1.1. Constitutive relation

The plate can be made of NC perfectly bonded orthotropic layers of the same material. Using matrix notation, the three dimensional constitutive law in the material coordinate is given by:

$$\boldsymbol{\sigma}_m = \widetilde{\mathbf{C}}\boldsymbol{\varepsilon}_m \tag{1}$$

where the stress vector $\boldsymbol{\sigma}_m$, the strain vector $\boldsymbol{\varepsilon}_m$ and $\widetilde{\mathbf{C}}$ are written in the material coordinate. $\widetilde{\mathbf{C}}$ is defined as:

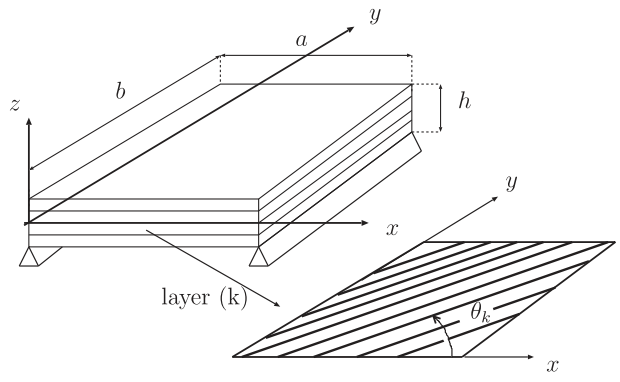

Fig. 1. Geometry of the plate and orientation of the fibers of the laminated plate.

$$\widetilde{\mathbf{C}} = \begin{bmatrix} \widetilde{C}_{11} & \widetilde{C}_{12} & \widetilde{C}_{13} & 0 & 0 & 0 \\ & \widetilde{C}_{22} & \widetilde{C}_{23} & 0 & 0 & 0 \\ & & \widetilde{C}_{33} & 0 & 0 & 0 \\ & & & \widetilde{C}_{44} & 0 & 0 \\ & sym & & & \widetilde{C}_{55} & 0 \\ & & & & & \widetilde{C}_{66} \end{bmatrix} \tag{2}$$

The stiffness coefficients $\widetilde{C}_{ij}$ are not reported for brevity reason (see [40] for more details). For each layer (k), a rotation matrix $\mathbf{R}^{(k)}$ is defined to obtain the constitutive law in the global coordinate system. So, we have:

$$\begin{bmatrix} \sigma_{11}^{(k)} \\ \sigma_{22}^{(k)} \\ \sigma_{33}^{(k)} \\ \sigma_{23}^{(k)} \\ \sigma_{13}^{(k)} \\ \sigma_{12}^{(k)} \end{bmatrix} = \begin{bmatrix} C_{11}^{(k)} & C_{12}^{(k)} & C_{13}^{(k)} & 0 & 0 & C_{16}^{(k)} \\ & C_{22}^{(k)} & C_{23}^{(k)} & 0 & 0 & C_{26}^{(k)} \\ & & C_{33}^{(k)} & 0 & 0 & C_{36}^{(k)} \\ & & & C_{44}^{(k)} & C_{45}^{(k)} & 0 \\ & sym & & & C_{55}^{(k)} & 0 \\ & & & & & C_{66}^{(k)} \end{bmatrix} \begin{bmatrix} \varepsilon_{11}^{(k)} \\ \varepsilon_{22}^{(k)} \\ \varepsilon_{33}^{(k)} \\ \gamma_{23}^{(k)} \\ \gamma_{13}^{(k)} \\ \gamma_{12}^{(k)} \end{bmatrix} \text{ i.e. } \boldsymbol{\sigma}^{(k)} = \mathbf{C}^{(k)}\boldsymbol{\varepsilon}^{(k)} \tag{3}$$

with $\mathbf{C}^{(k)} = \mathbf{R}^{(k)}\widetilde{\mathbf{C}}\mathbf{R}^{(k)^T}$

and

$$\mathbf{R}^{(k)} = \begin{bmatrix} \cos^2\theta_k & \sin^2\theta_k & 0 & 0 & 0 & -2\sin\theta_k\cos\theta_k \\ \sin^2\theta_k & \cos^2\theta_k & 0 & 0 & 0 & 2\sin\theta_k\cos\theta_k \\ 0 & 0 & 1 & 0 & 0 & 0 \\ 0 & 0 & 0 & \cos\theta_k & \sin\theta_k & 0 \\ 0 & 0 & 0 & -\sin\theta_k & \cos\theta_k & 0 \\ \sin\theta_k\cos\theta_k & -\sin\theta_k\cos\theta_k & 0 & 0 & 0 & \cos^2\theta_k - \sin^2\theta_k \end{bmatrix} \tag{4}$$

We denote the stress vector $\boldsymbol{\sigma}^{(k)}$, the strain vector $\boldsymbol{\varepsilon}^{(k)}$, the fibers orientation θ_k (Fig. 1) and $C_{ij}^{(k)}$ the three-dimensional stiffness coefficients of the layer (k) in the global coordinate system.

2.1.2. The classical weak form of the boundary value problem

The plate is submitted to a surface force density $\mathbf{t}$ defined over a subset Γ_N of the boundary and a body force density $\mathbf{b}$ defined in Ω. We assume that a prescribed displacement $\mathbf{u} = \mathbf{u}_d$ is imposed on $\Gamma_D = \partial\Omega - \Gamma_N$.

The classical formulation of the elastic problem is recalled: find a displacement field $\mathbf{u}$ and a stress field $\boldsymbol{\sigma}$ defined in $\mathcal{V}$ which verify:

- the kinematic constraints:

$$\mathbf{u} \in \mathcal{U} \tag{5}$$

- the equilibrium equations:

$$\boldsymbol{\sigma} \in \mathcal{S} \text{ and } \forall \mathbf{u}^* \in \mathcal{U}^* \quad -\int_{\mathcal{V}} \boldsymbol{\sigma} : \boldsymbol{\varepsilon}(\mathbf{u}^*)\, d\mathcal{V} + \int_{\mathcal{V}} \mathbf{b}.\mathbf{u}^*\, d\mathcal{V} + \int_{\Gamma_N} \mathbf{t}.\mathbf{u}^* d\Gamma = 0 \tag{6}$$

- the constitutive relation:

$$\boldsymbol{\sigma} = \mathbf{C}\boldsymbol{\varepsilon}(\mathbf{u}) \tag{7}$$

$\mathcal{U} = \{\mathbf{u} | \mathbf{u} \in (\mathcal{H}^1(\mathcal{V}))^3; \mathbf{u} = \mathbf{u}_d \text{ on } \Gamma_D\}$ is the space in which the displacement field is being sought, $\mathcal{S} = \mathcal{L}^2[\mathcal{V}]^3$ the space of the stresses, and $\boldsymbol{\varepsilon}(\mathbf{u})$ denotes the linearized strain associated with the displacement.

3. Application of the Proper Generalized Decomposition to plate with any stacking sequences

The Proper Generalized Decomposition (PGD) was introduced in [33] and is based on an *a priori* construction of separated variables

representation of the solution. The following sections are dedicated to the introduction of the PGD to build a parametric solution for composite plate with any stacking sequences. An illustration is proposed in [37]. We consider the problem defined by Eqs. (5)–(7) as a parametrized problem where the orientation of each ply θ_k is in a bounded interval $\mathcal{I}_k = [\theta_m^k; \theta_M^k]$. The solution of Eqs. (5)–(7) for a point M of the structure depends on the values of these angles and is denoted $\mathbf{u}(M, \theta_1, \theta_2, \dots \theta_{NC})$, and the stress is linked with the strain by a parametrized constitutive law $\mathbf{C}^{(\mathbf{k})}(\boldsymbol{\theta}_\mathbf{k})$.

3.1. The parametrized problem

The displacement solution $\mathbf{u}$ is constructed as the sum of N products of separated functions ($N \in \mathbb{N}$ is the order of the representation)

$$\mathbf{u}(x,y,z,\theta_1,\theta_2,\dots\theta_{NC}) = \sum_{i=1}^{N} g_1^i(\theta_1) g_2^i(\theta_2) \dots g_{NC}^i(\theta_{NC})\, \mathbf{f}^\mathbf{i}(z) \circ \mathbf{v}^i(x,y) \tag{8}$$

where $g_k^i(\theta_k)$, $\mathbf{f}^\mathbf{i}(z)$ and $\mathbf{v}^i(x,y)$ are unknown functions which must be computed during the resolution process. $g_k^i(\theta_k)$, $\mathbf{f}^\mathbf{i}(z)$ and $\mathbf{v}^i(x,y)$ are defined on $\mathcal{I}_k$, Ω_z and Ω respectively. The "$\circ$" operator in Eq. (8) is Hadamard's element-wise product. We have:

$$\mathbf{f}^i \circ \mathbf{v}^i = \mathbf{v}^i \circ \mathbf{f}^i = \begin{bmatrix} f_1^i(z)\, v_1^i(x,y) \\ f_2^i(z)\, v_2^i(x,y) \\ f_3^i(z)\, v_3^i(x,y) \end{bmatrix} \text{ with } \mathbf{v}^i = \begin{bmatrix} v_1^i(x,y) \\ v_2^i(x,y) \\ v_3^i(x,y) \end{bmatrix} \mathbf{f}^i = \begin{bmatrix} f_1^i(z) \\ f_2^i(z) \\ f_3^i(z) \end{bmatrix} \tag{9}$$

Note that the in-plane coordinates and the transverse coordinate are separated in the expression of the displacements as in [38].

For sake of clarity, the body forces are neglected in the developments and the new problem to be solved is written as follows: find $\mathbf{u} \in \mathcal{U}$ (space of admissible displacements) such that

$$a(\mathbf{u}, \mathbf{u}^*) = b(\mathbf{u}^*)\ \forall \mathbf{u}^* \in \mathcal{U}^* \tag{10}$$

with

$$\begin{aligned} a(\mathbf{u}, \mathbf{u}^*) &= \int_{\Omega\times\Omega_z\times\mathcal{I}_1\times\mathcal{I}_2\dots\times\mathcal{I}_{NC}} \mathbf{C}\boldsymbol{\varepsilon}(\mathbf{u}) : \boldsymbol{\varepsilon}(\mathbf{u}^*)\, d\Omega\, d\Omega_z\, d\theta_1 \dots d\theta_{NC} \\ b(\mathbf{u}^*) &= \int_{\Gamma_N\times\mathcal{I}_1\times\mathcal{I}_2\dots\times\mathcal{I}_{NC}} \mathbf{t}.\mathbf{u}^* d\Gamma\, d\theta_1 \dots d\theta_{NC} \end{aligned} \tag{11}$$

where $\Omega \times \Omega_z \times \mathcal{I}_1 \times \mathcal{I}_2 \dots \times \mathcal{I}_{NC}$ is the integration space associated with the geometric space domain $\Omega \times \Omega_z$ and the parameters domain of the laminae orientation $\mathcal{I}_1 \times \mathcal{I}_2 \dots \times \mathcal{I}_{NC}$. For the present work, Γ_N is considered as the top or bottom surfaces of the plate, that is $z = z_F$ with $z_F = \pm h/2$.

The strain derived from Eq. (8) is

$$\boldsymbol{\varepsilon}(u) = \sum_{i=1}^{N} g_1^i(\theta_1) g_2^i(\theta_2) \dots g_{NC}^i(\theta_{NC}) \begin{bmatrix} f_1^i\, v_{1,1}^i \\ f_2^i\, v_{2,2}^i \\ (f_3^i)'\, v_3^i \\ (f_2^i)'\, v_2^i + f_3^i\, v_{3,2}^i \\ (f_1^i)'\, v_1^i + f_3^i\, v_{3,1}^i \\ f_1^i\, v_{1,2}^i + f_2^i\, v_{2,1}^i \end{bmatrix} \tag{12}$$

where the prime stands for the classical derivative $\left(f_i' = \frac{df_i}{dz}\right)$, and $()_{,\alpha}$ for the partial derivative. The dependance with respect to the space coordinates is omitted.

3.2. decomposition of the parametrized problem

We assume that a sum of $n < N$ products of separated functions have been already computed. Therefore, we have:

$$\mathbf{u}^n(x,y,z,\theta_1,\theta_2,\dots\theta_{NC}) = \sum_{i=1}^{n} g_1^i(\theta_1) g_2^i(\theta_2) \dots g_{NC}^i(\theta_{NC}) \mathbf{f}^\mathbf{i}(z) \circ \mathbf{v}^i(x,y) \tag{13}$$

and the solution at step $n+1$ is sought as the sum of $\mathbf{u}^n$ and a product $g_1^{n+1}(\theta_1) g_2^{n+1}(\theta_2) \dots g_{NC}^{n+1}(\theta_{NC})\, \mathbf{f}^{\mathbf{n+1}}(z) \circ \mathbf{v}^{n+1}(x,y)$ of unknown functions. So, $\mathbf{u}^{n+1}$ can be written as

$$\begin{aligned} \mathbf{u}^{n+1}(x,y,z,\theta_1,\theta_2,\dots\theta_{NC}) &= \mathbf{u}^n(x,y,z,\theta_1,\theta_2,\dots\theta_{NC}) \\ &+ g_1^{n+1}(\theta_1) g_2^{n+1}(\theta_2) \dots g_{NC}^{n+1}(\theta_{NC})\, \mathbf{f}^{\mathbf{n+1}}(z) \circ \mathbf{v}^{n+1}(x,y) \end{aligned} \tag{14}$$

Let us denote by $\mathbf{g}^{n+1}$ the set of functions $(g_1^{n+1}, g_2^{n+1}, \dots g_{NC}^{n+1})$ and by $\pi_i(\mathbf{g})$ and $\pi(\mathbf{g})$ the two following products

$$\pi_i(\mathbf{g}) = \prod_{\substack{j=1 \\ j\neq i}}^{NC} g_j \text{ and } \pi(\mathbf{g}) = \prod_{j=1}^{NC} g_j \tag{15}$$

The test functions are derived from Eq. (14)

$$\begin{aligned} \mathbf{u}^* = \sum_{i=1}^{NC} \pi_i(\mathbf{g}^{n+1}) g_i^*\, \mathbf{f}^{n+1} \circ \mathbf{v}^{n+1} + \pi(\mathbf{g}^{n+1})\, \mathbf{v}^{n+1} \circ \mathbf{f}^* \\ + \pi(\mathbf{g}^{n+1})\, \mathbf{f}^{n+1} \circ \mathbf{v}^* \end{aligned} \tag{16}$$

Introducing the trial function $\mathbf{u}$ defined by Eq. (14) and the test functions $\mathbf{u}^*$ defined by Eq. (16) into the weak form (Eq. (10)) leads to the $NC+2$ following equations, where the unknown functions $g_i^{n+1}(\theta_i)$, $\mathbf{g}^{n+1}$, $\mathbf{f}^{n+1}(z)$, $\mathbf{v}^{n+1}(x,y)$ are denoted g_i, $\mathbf{g}$, $\mathbf{f}$, $\mathbf{v}$ for sake of clarity:

- for the test functions g_i^*, $i \in \{1, \dots, NC\}$

$$\begin{aligned} &a\left(\pi_i(\mathbf{g}) g_i\, \mathbf{f} \circ \mathbf{v}, \pi_i(\mathbf{g}) g_i^*\, \mathbf{f} \circ \mathbf{v}\right) \\ &\quad = b\left(\pi_i(\mathbf{g})\, \mathbf{f} \circ \mathbf{v} g_i^*\right) - a\left(\mathbf{u}^n, \pi_i(\mathbf{g}) g_i^*\, \mathbf{f} \circ \mathbf{v}\right) \quad \forall g_i^* \end{aligned} \tag{17}$$

- for the test function $\mathbf{f}^*$

$$\begin{aligned} a(\pi(\mathbf{g})\, \mathbf{v} \circ \mathbf{f}, \pi(\mathbf{g})\, \mathbf{v} \circ \mathbf{f}^*) &= b(\pi(\mathbf{g})\, \mathbf{v} \circ \mathbf{f}^*) \\ &- a(\mathbf{u}^n, \pi(\mathbf{g})\, \mathbf{v} \circ \mathbf{f}^*) \quad \forall \mathbf{f}^* \end{aligned} \tag{18}$$

- for the test function $\mathbf{v}^*$

$$\begin{aligned} a(\pi(\mathbf{g})\, \mathbf{f} \circ \mathbf{v}, \pi(\mathbf{g})\, \mathbf{f} \circ \mathbf{v}^*) &= b(\pi(\mathbf{g})\, \mathbf{f} \circ \mathbf{v}^*) \\ &- a(\mathbf{u}^n, \pi(\mathbf{g})\, \mathbf{f} \circ \mathbf{v}^*) \quad \forall \mathbf{v}^* \end{aligned} \tag{19}$$

As these equations define a coupled non-linear system, a non-linear resolution strategy has to be used. The fixed point method is used. Starting from an initial solution $(\tilde{\mathbf{g}}^{(0)}, \tilde{\mathbf{f}}^{(0)}, \tilde{\mathbf{v}}^{(0)})$, we construct a sequence $(\tilde{\mathbf{g}}^{(j)})_{j\geqslant 1}, (\tilde{\mathbf{f}}^{(j)})_{j\geqslant 1}$ and $(\tilde{\mathbf{v}}^{(j)})_{j\geqslant 1}$ which satisfy Eqs. (17)–(19) respectively. For each problem involving one unknown function, the two other ones are supposed to be known and come from the previous step of the fixed point strategy. So, the PGD leads to the algorithm given in Table 1.

In practice, only few iterations of the fixed point algorithm are necessary to reach a good approximation $(\tilde{\mathbf{f}}^{(j)}, \tilde{\mathbf{v}}^{(j)}, \tilde{\mathbf{g}}^{(j)})$ of $(\mathbf{f}^{n+1}, \mathbf{v}^{n+1}, \mathbf{g}^{n+1})$ (see [41] for more details).

Table 1
Proper Generalized Decomposition algorithm.

- for $n = 1$ to N_{max}
  Initialize $\tilde{\mathbf{f}}^{(0)}$, $\tilde{\mathbf{v}}^{(0)}$ and $\tilde{\mathbf{g}}_i^{(0)}$ for $i \in \{1, \dots NC\}$
  for $j = 1$ to j_{max}
    for $i = 1$ to NC
      Compute $\tilde{\mathbf{g}}_i^{(j)}$ from Eq. (17), $\tilde{\mathbf{g}}_p^{(j)}$ $(p < i)$, $\tilde{\mathbf{g}}_p^{(j-1)}$ $(p > i)$, $\tilde{\mathbf{f}}^{(j-1)}$ and $\tilde{\mathbf{v}}^{(j-1)}$ being known
    end for
    Compute $\tilde{\mathbf{f}}^{(j)}$ from Eq. (18), $\tilde{\mathbf{g}}^{(j)}$ and $\tilde{\mathbf{v}}^{(j-1)}$ being known
    Compute $\tilde{\mathbf{v}}^{(j)}$ from Eq. (19), $\tilde{\mathbf{g}}^{(j)}$ and $\tilde{\mathbf{f}}^{(j)}$ being known
    Check for convergence
  end for
  Set $\mathbf{f}^{n+1} = \tilde{\mathbf{f}}^{(j)}$, $\mathbf{v}^{n+1} = \tilde{\mathbf{v}}^{(j)}$ and $\mathbf{g}^{n+1} = \tilde{\mathbf{g}}^{(j)}$
  Set $\mathbf{u}^{n+1} = \mathbf{u}^n + \pi(\mathbf{g}^{n+1})\mathbf{f}^{n+1} \circ \mathbf{v}^{n+1}$
  Check for convergence
- end for

3.3. discretization

To compute the solution of Eqs. (17)–(19), a discrete representation of the functions $(\mathbf{f}, \mathbf{v}, g_1, \dots g_{NC})$ must be introduced. We use a classical finite element approximation in Ω, and a polynomial expansion in Ω_z for $\mathbf{v}$ and $\mathbf{f}$ respectively. The elementary vector of degrees of freedom (dof) associated with one element Ω_e of the mesh in Ω is denoted $\mathbf{q}_e^v$. The vector of dofs associated with the polynomial expansion in Ω_z is denoted $\mathbf{q}^f$. The displacement fields and the strain fields are determined from the values of $\mathbf{q}_e^v$ and $\mathbf{q}^f$ by

$$\mathbf{v}_e = \mathbf{N}_{xy}\mathbf{q}_e^v, \quad \boldsymbol{\mathcal{E}}_v^e = \mathbf{B}_{xy}\mathbf{q}_e^v, \quad \mathbf{f} = \mathbf{N}_z\mathbf{q}^f \quad \text{and} \quad \boldsymbol{\mathcal{E}}_f = \mathbf{B}_z\mathbf{q}^f \tag{20}$$

The matrices $\mathbf{N}_{xy}$, $\mathbf{B}_{xy}$, $\mathbf{N}_z$, $\mathbf{B}_z$ contain the interpolation functions, their derivatives and the jacobian components. $\boldsymbol{\mathcal{E}}_v^e$ and $\boldsymbol{\mathcal{E}}_f$ are defined in Appendices A and B, respectively.

As far as the functions $g_1, \dots, g_{NC}$ are concerned, a piecewise linear interpolation is considered in $(\mathcal{I}_k)_{1 \leqslant k \leqslant NC}$

$$g_k(\theta_k) = \mathbf{N}_{g_k}(\theta_k)\mathbf{q}^{g_k} \tag{21}$$

where $\mathbf{N}_{g_k}$ is the matrix of the interpolation functions, $\mathbf{q}^{g_k}$ are the degree of freedom.

3.3.1. Finite element problem to be solved on $\mathcal{I}_k$

For the sake of simplicity, the functions $\tilde{\mathbf{f}}^{(j-1)}$, $\tilde{\mathbf{v}}^{(j-1)}$ and $\left(\tilde{g}_i^{(j)}\right)_{1 \leqslant i \leqslant NC,\ i \neq k}$ which are assumed to be known, will be denoted $\tilde{\mathbf{f}}$, $\tilde{\mathbf{v}}$ and $\tilde{\mathbf{g}}_{\setminus k} = (g_i)_{1 \leqslant i \leqslant NC,\ i \neq k}$, and the function $\tilde{g}_k^{(j)}$ to be computed will be denoted g_k.

The variational problem defined on $\mathcal{I}_k$ from Eq. (17) is

$$\int_{\mathcal{I}_k} g_k^* k_{kxyz}(\tilde{\mathbf{g}}_{\setminus k}, \tilde{\mathbf{f}}, \tilde{\mathbf{v}}) g_k d\theta_k = \int_{\mathcal{I}_k} g_k^* t_{kxyz}(\tilde{\mathbf{g}}_{\setminus k}, \tilde{\mathbf{f}}, \tilde{\mathbf{v}}) d\theta_k - \int_{\mathcal{I}_k} g_k^* \sigma_{kxyz}(\tilde{\mathbf{g}}_{\setminus k}, \tilde{\mathbf{f}}, \tilde{\mathbf{v}}, \mathbf{u}^n) d\theta_k \tag{22}$$

$$k_{kxyz}(\tilde{\mathbf{g}}_{\setminus k}, \tilde{\mathbf{f}}, \tilde{\mathbf{v}}) = \int_{\Omega \times \Omega_z \times \mathcal{I}_{\setminus k}} \left[\boldsymbol{\varepsilon}(\tilde{\mathbf{f}} \circ \tilde{\mathbf{v}})^T \mathbf{C} \boldsymbol{\varepsilon}(\tilde{\mathbf{f}} \circ \tilde{\mathbf{v}}) \prod_{\substack{i=1 \\ i \neq k}}^{NC} \tilde{g}_i^2 \right] d\Omega dz d\theta_1 \dots d\theta_{NC} \tag{23}$$

$$t_{kxyz}(\tilde{\mathbf{g}}_{\setminus k}, \tilde{\mathbf{f}}, \tilde{\mathbf{v}}) = \int_{\Omega \times \mathcal{I}_{\setminus k}} \left[(\tilde{\mathbf{f}} \circ \tilde{\mathbf{v}})^T \mathbf{t} \pi_k(\tilde{\mathbf{g}}) \right] d\Omega d\theta_1 \dots d\theta_{NC} \Big|_{z=z_F} \tag{24}$$

$$\sigma_{kxyz}(\tilde{\mathbf{g}}_{\setminus k}, \tilde{\mathbf{f}}, \tilde{\mathbf{v}}, \mathbf{u}^n) = \int_{\Omega \times \Omega_z \times \mathcal{I}_{\setminus k}} \left[\boldsymbol{\varepsilon}(\tilde{\mathbf{f}} \circ \tilde{\mathbf{v}})^T \mathbf{C} \boldsymbol{\varepsilon}(\mathbf{u}^n)\, \pi_k(\tilde{\mathbf{g}}) \right] d\Omega dz d\theta_1 \dots d\theta_{NC} \tag{25}$$

with $\mathcal{I}_{\setminus k} = \mathcal{I}_1 \times \mathcal{I}_2 \dots \times \mathcal{I}_{k-1} \times \mathcal{I}_{k+1} \dots \times \mathcal{I}_{NC}$

Note that the domain of integration in Eqs. (23)–(25) can be splitted into the parameters domains and the geometric space domain.

The introduction of the finite element approximation Eq. (21) in the variational Eq. (22) leads to the linear system

$$\mathbf{K}_{kxyz}(\tilde{\mathbf{g}}_{\setminus k}, \tilde{\mathbf{f}}, \tilde{\mathbf{v}})\mathbf{q}^{g_k} = \mathcal{R}_{g_k}(\tilde{\mathbf{g}}_{\setminus k}, \tilde{\mathbf{f}}, \tilde{\mathbf{v}}, \mathbf{u}^n) \tag{26}$$

where

- $\mathbf{q}^{g_k}$ is the vector of dofs associated with the expansion in $\mathcal{I}_k$,
- $\mathbf{K}_{kxyz}(\tilde{\mathbf{g}}_{\setminus k}, \tilde{\mathbf{f}}, \tilde{\mathbf{v}})$ is the stiffness matrix obtained by

$$\mathbf{K}_{kxyz}(\tilde{\mathbf{g}}_{\setminus k}, \tilde{\mathbf{f}}, \tilde{\mathbf{v}}) = \int_{\mathcal{I}_k} \mathbf{N}_{g_k}^T k_{kxyz}(\tilde{\mathbf{g}}_{\setminus k}, \tilde{\mathbf{f}}, \tilde{\mathbf{v}}) \mathbf{N}_{g_k} d\theta_k$$

- $\mathcal{R}_{g_k}(\tilde{\mathbf{g}}_{\setminus k}, \tilde{\mathbf{f}}, \tilde{\mathbf{v}}, \mathbf{u}^n)$ is the equilibrium residual obtained by

$$\mathcal{R}_{g_k}(\tilde{\mathbf{g}}_{\setminus k}, \tilde{\mathbf{f}}, \tilde{\mathbf{v}}, \mathbf{u}^n) = \int_{\mathcal{I}_k} \mathbf{N}_{g_k}^T t_{kxyz}(\tilde{\mathbf{g}}_{\setminus k}, \tilde{\mathbf{f}}, \tilde{\mathbf{v}}) d\theta_k - \int_{\mathcal{I}_k} \mathbf{N}_{g_k}^T \sigma_{kxyz}(\tilde{\mathbf{g}}_{\setminus k}, \tilde{\mathbf{f}}, \tilde{\mathbf{v}}, \mathbf{u}^n) d\theta_k$$

3.3.2. Finite element problem to be solved on Ω and Ω_z

The Finite Element problems on Ω and Ω_z are a straightforward extension of the formulation given in [38] to the parametrized problem involving θ_k. However, for the sake of completeness, their formulations are given in Appendices A and B.

4. Numerical results

In this section, an eight-node quadrilateral FE based on the classical Serendipity interpolation functions [10] is used for the unknowns depending on the in-plane coordinates. A Gaussian numerical integration with 3×3 points is used to evaluate the elementary matrices. A fourth-order Layerwise z-expansion is also considered. Concerning the functions associated to the orientations of the plies θ_k, a piecewise linear function is chosen. An analytical integration of the functions with respect to θ_k and the transverse coordinate is performed. In the following, the plate is discretized with $N_x \times N_y$ elements. The total number of numerical layer is denoted N_z. The numbers of dofs are also precised for the three problems associated to $(g_j{}^n)_{1 \leqslant j \leqslant NC}$, $\mathbf{v}^n$ and $\mathbf{f}^n$. They are denoted $Ndof_{\theta_j}$, $Ndof_{xy}$ and $Ndof_z$ respectively.

First, a one-layer plate is considered to show the accuracy of the method. The influence of the discretization of the function $g_1(\theta_1)$ is studied. Then, the method is assessed on two and four-layer plate configurations. The results are compared with reference results issued from PGD computations without introducing the laminae orientations as parameters. Indeed, the performance of this latter

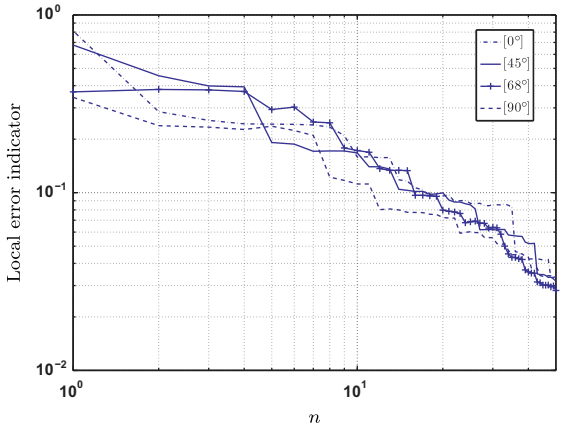

Fig. 2. Local error indicator with respect to the PGD iterations – $S = 4$ – 1 layer – $\theta_1 \in [-90, 90]$.

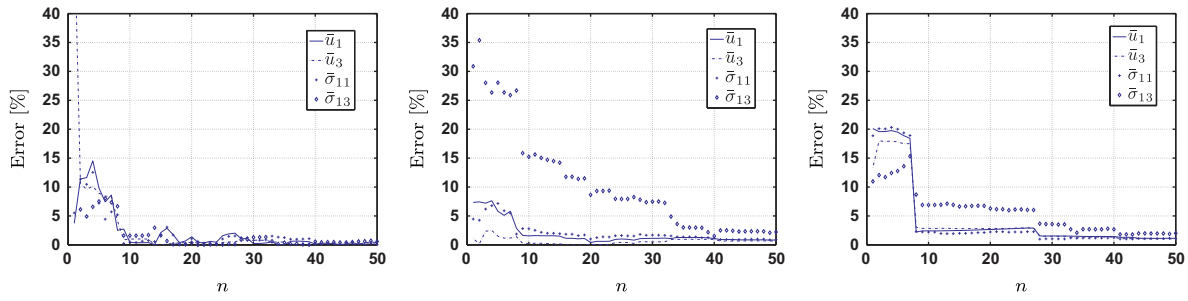

Fig. 3. Error on the maximal values of $\bar{u}$, $\bar{w}$, $\bar{\sigma}_{11}$ and $\bar{\sigma}_{13}$ with respect to the PGD iterations – $[0^\circ]$ (left), $[68^\circ]$ (middle), $[90^\circ]$ (right) – $S = 4$ – 1 layer – $\theta_1 \in [-90^\circ, 90^\circ]$.

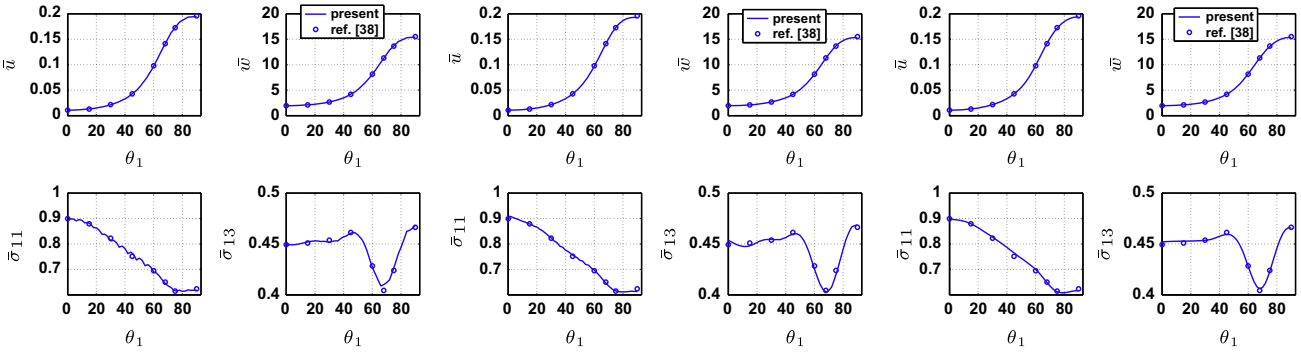

Fig. 4. Distribution of $\max(\bar{u})$, $\max(\bar{w})$, $\max(\bar{\sigma}_{11})$, and $\max(\bar{\sigma}_{13})$ with respect to the orientation θ_1 – $Ndof_{\theta_1} = 30$ (left), 50 (middle), 150 (right) – $S = 4$ – 1 layer – $\theta_1 \in [-90^\circ, 90^\circ]$.

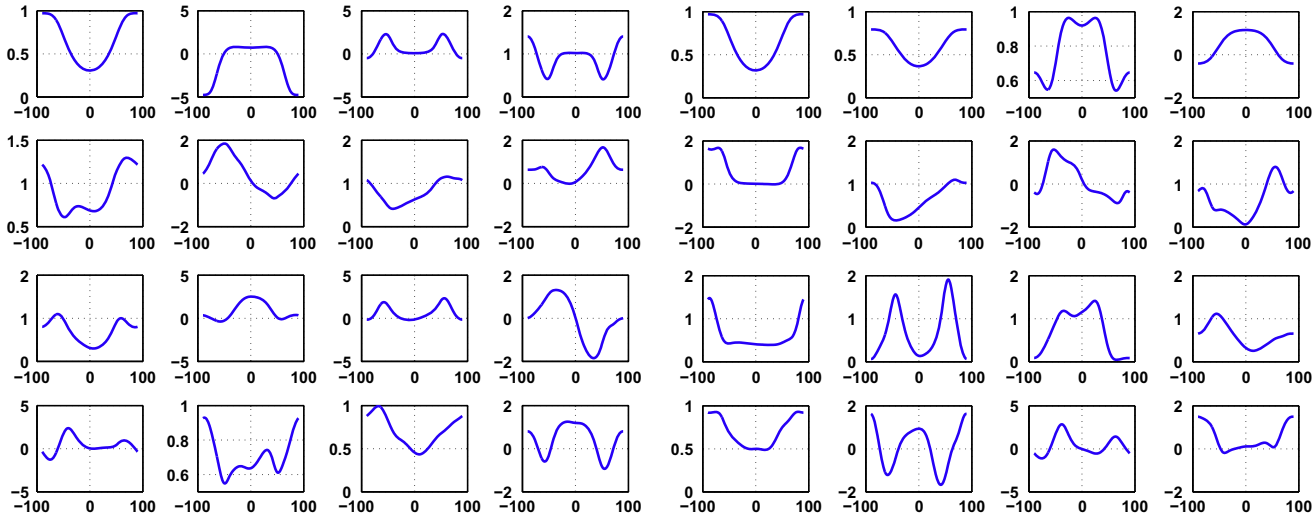

Fig. 5. 16 First functions $g_i(\theta_i)$ – $S = 4$ – 2 layers – $\theta_i \in [-90, 90]$, $i = 1, 2$.

has been shown in [38] and can be considered as a reference solution.

All the following tests involve a simply-supported plate submitted to a sinusoidal pressure. They are described below:

geometry: rectangular composite plate with $b = 3a$. All layers have the same thickness $S = \frac{a}{h} = 4$.
boundary conditions: cylindrical bending of a plate submitted to a sinusoidal pressure $q(x, y) = q_0 \sin\frac{\pi x}{a}$.
material properties: $E_L = 25$ GPa, $E_T = 1$ GPa, $G_{LT} = 0.2$ GPa, $G_{TT} = 0.5$ GPa, $\nu_{LT} = \nu_{TT} = 0.25$ where L refers to the fiber direction, T refers to the transverse direction.
mesh: $N_x = N_y = 16$ and the whole plate is meshed.
number of dofs: $Ndof_{xy} = 2499$ and $Ndof_z = 3(4 \times NC + 1)$.
results: The results are made non-dimensional using:

$$\bar{u} = u_1(0, b/2, z)\frac{E_T}{hq_0S^3}, \quad \bar{w} = u_3(a/2, b/2, z)\frac{100E_T}{S^4hq_0}$$

$$\bar{\sigma}_{\alpha\alpha} = \frac{\sigma_{\alpha\alpha}(a/2, b/2, z)}{q_0S^2}, \quad \bar{\sigma}_{12} = \frac{\sigma_{12}(0, 0, z)}{q_0S^2}$$

$$\bar{\sigma}_{13} = \frac{\sigma_{13}(0, b/2, z)}{q_0S}, \quad \bar{\sigma}_{zz} = \frac{\sigma_{zz}(a/2, b/2, z)}{q_0}$$

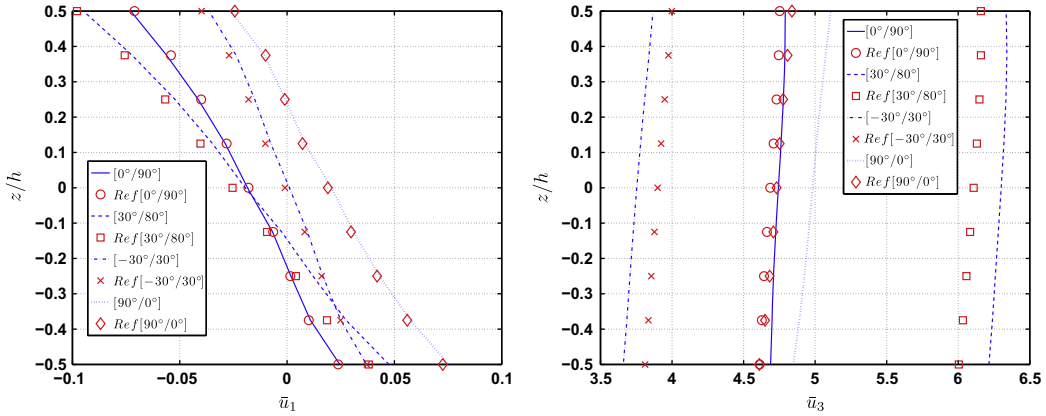

Fig. 6. Distribution of $\bar{u}_1$ (left) and $\bar{u}_3$ (right) along the thickness – $S = 4$ – 2 layers – $[0°/90°]$, $[30°/80°]$, $[-30°/30°]$ and $[90°/0°]$ – $\theta_1 \in [-90, 90]$, $\theta_2 \in [-90, 90]$.

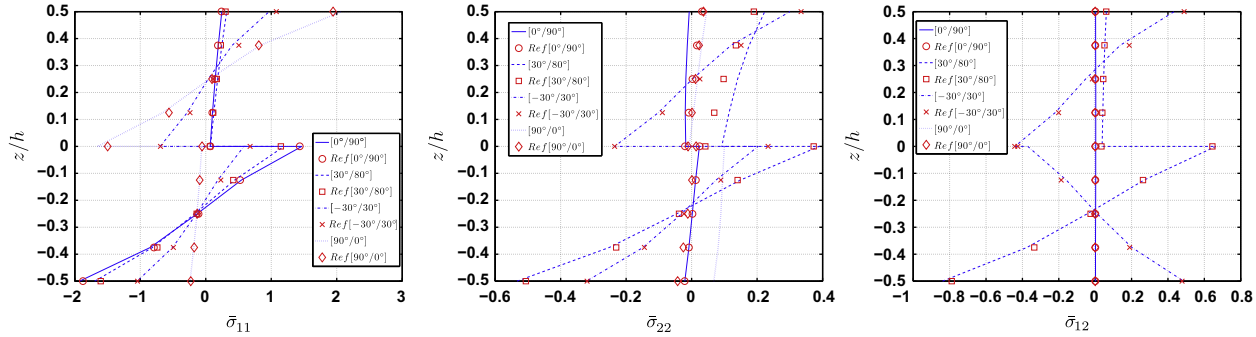

Fig. 7. Distribution of $\bar{\sigma}_{11}$ (left), $\bar{\sigma}_{22}$ (middle) and $\bar{\sigma}_{12}$ (right) along the thickness – $S = 4$ – 2 layers – $[0°/90°]$, $[30°/80°]$, $[-30°/30°]$ and $[90°/0°]$ – $\theta_1 \in [-90, 90]$, $\theta_2 \in [-90, 90]$.

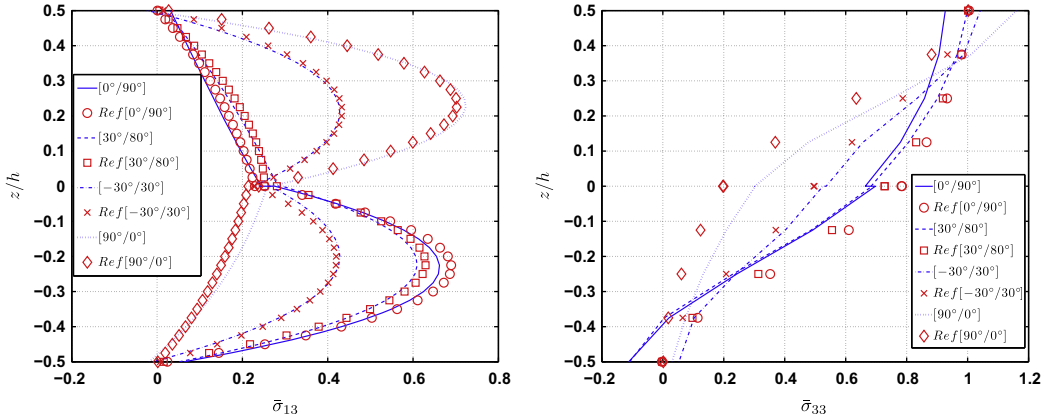

Fig. 8. Distribution of $\bar{\sigma}_{13}$ (left) and $\bar{\sigma}_{33}$ (right) along the thickness – $S = 4$ – 2 layers – $[0°/90°]$, $[30°/80°]$, $[-30°/30°]$ and $[90°/0°]$ – $\theta_1 \in [-90, 90]$, $\theta_2 \in [-90, 90]$.

4.1. One-layered plate

The approach is first assessed on a one-layered plate where the orientation of the ply belongs to the interval $\mathcal{I}_1 = [-90°, 90°]$. It allows us to consider the most general case. For a fixed value of θ_1, a local error indicator between a reference solution $\mathbf{u}^{ref}$ and a separated variables solution $\mathbf{u}^n$ of order n is introduced as

$$\epsilon_n = \sqrt{\frac{a_{err}(\mathbf{u}^n - \mathbf{u}^{ref}, \mathbf{u}^n - \mathbf{u}^{ref})}{a_{err}(\mathbf{u}^{ref}, \mathbf{u}^{ref})}} \quad \text{with } a_{err}(\mathbf{u}, \mathbf{v}) = \int_{\Omega \times \Omega_z} \mathbf{C}\boldsymbol{\varepsilon}(\mathbf{u}) : \boldsymbol{\varepsilon}(\mathbf{v})\, d\Omega\, d\Omega_z \tag{27}$$

The variation of this error indicator with respect to the number of PGD iterations is represented on Fig. 2 for $\theta_1 = 0°, 45°, 68°, 90°$. The trend of these four configurations is rather similar. For further investigations, Fig. 3 shows the error rate on the maximum values of displacements and stresses along with the number of couples for different orientations. These errors are computed with respect to the PGD results using the fixed value of θ_1 [38]. Only few couples allow to decrease significantly the error rate for the three values of θ_1. Then, the convergence rate is slower. Nevertheless, the accuracy of the results is very satisfactory. For $n = 40$ couples, the error rate is less than 2.5% for both displacements and stresses. We also notice that the convergence rate is higher for the stiffest case (i.e. $\theta_1 = 0°$). Moreover, it can be inferred from this figure that the estimation of the transverse shear stress is the most expensive, while only 10

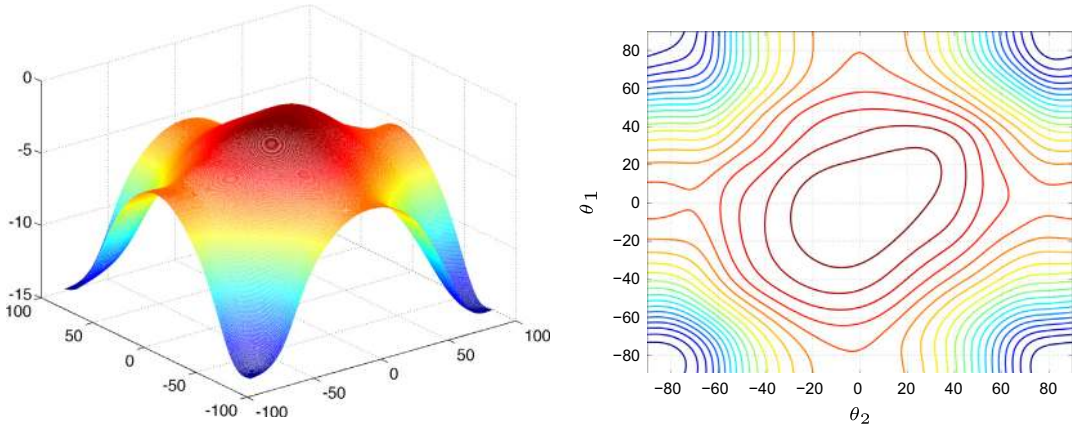

Fig. 9. $w(\theta_1, \theta_2)$ – $S = 4$ – 2 layers – $\theta_1 \in [-90, 90]$, $\theta_2 \in [-90, 90]$.

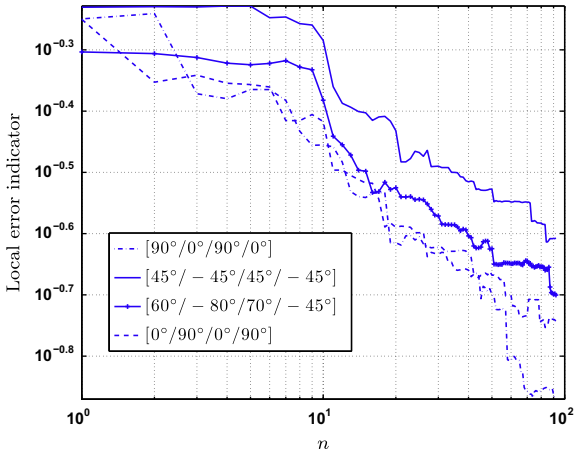

Fig. 10. Local error indicator – $S = 4$ – 4 layers – $\theta_i \in [-90, 90]$, $i = 1, 2, 3, 4$.

couples are needed to recover displacements with an error of less than 2.8%.

Once the computation is completed, the approach gives directly the explicit solution with respect to the orientation of the ply. Fig. 4 presents the variation of the in-plane, transverse displacements, the in-plane and transverse shear stresses with respect to this parameter θ_1 on the interval $[-90°, 90°]$ for different values of $Ndof_{\theta_1}$. Due to the symmetry, only the interval $[0°, 90°]$ is presented in Fig. 4. The results are compared with the reference solution [38] using eight fixed values of θ_1 (circle symbols on Fig. 4). On the one hand, this figure illustrates the accuracy and the interest of the present approach. On the other hand, the influence of the discretisation of the function g_1 is shown. From Fig. 4, $Ndof_{\theta_1} = 150$ seems to be sufficient to approximate the solution on the whole interval $[-90°, 90°]$ and to recover the extrema. Only $Ndof_{\theta_1} = 30$ is needed if the quantity of interest is the displacement.

Finally, we show that the parametrized solution obtained from the PGD algorithm allows us to represent the variation of displacements and stresses for a wide range of θ. We can deduce for instance that the minimal value of the transverse shear stress occurs for a value of θ_1 of around 68° for this case.

4.2. 2-layered plate

A two-layered case is carried out with $\mathcal{I}_i = [-90°, 90°]$, $i = 1, 2$, which allow us to consider all stacking sequences. For illustration, the sixteen first functions $g_i(\theta_i)$, $i = 1, 2$ are given in Fig. 5. All the displacements and stresses are presented in Figs. 6–8. Four different stacking sequences are shown and the results issued from the PGD are compared with reference solution, denoted $Ref[\theta_1, \theta_2]$. 50 couples are needed to obtain the solution. We notice that the results are rather accurate with respect to the reference regardless of the configurations. For the transverse shear stress, the maximum value is well-estimated. The distribution of the transverse normal stress which is the most difficult to compute is rather correct.

Owing to the explicit solution, the influence of the orientation of the two plies on the transverse displacement can be easily shown (Cf. Fig. 9). The stiffest and the most flexible configurations

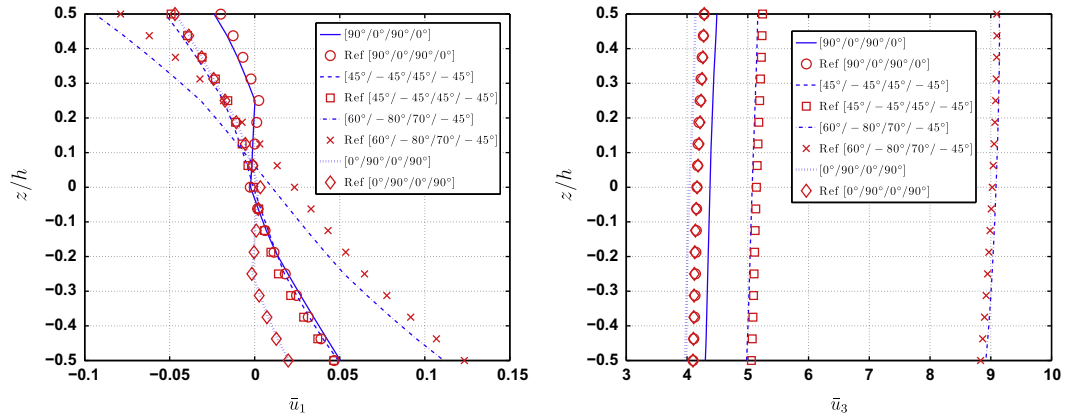

Fig. 11. Distribution of $\bar{u}_1$ (left) and $\bar{u}_3$ (right) along the thickness – $S = 4$ – 4 layers – $\theta_i \in [-90, 90]$.

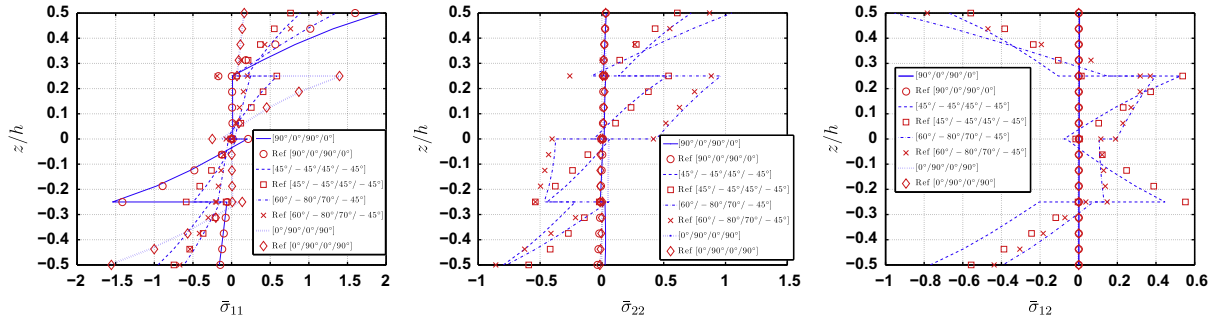

Fig. 12. Distribution of $\bar{\sigma}_{11}$ (left), $\bar{\sigma}_{22}$ (middle) and $\bar{\sigma}_{12}$ (right) along the thickness – $S = 4$ – 4 layers – $\theta_i \in [-90, 90]$.

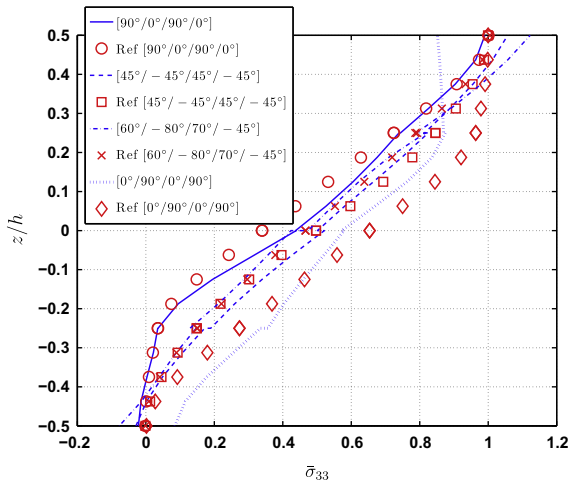

Fig. 13. Distribution of $\bar{\sigma}_{33}$ along the thickness – $S = 4$ – 4 layers – $\theta_i \in [-90, 90]$.

can be deduced. A ratio of five between these ones can be estimated.

4.3. 4-layered plate

A 4-layered plate is now considered to increase the number of layers and assess the present approach. Fig. 10 illustrates the convergence of the PGD algorithm for four stacking sequences with the local error indicator introduced in Eq. (27). 92 couples are built to compute the solution. For further assessment, the distributions of the in-plane and transverse displacements, the in-plane, transverse shear and normal stresses are shown in Figs. 11–14. It can again be inferred from these figures that the results are in good agreement with the reference solution. In particular, the distribution of the transverse shear stress which can be completely different for various stacking sequences is rather well estimated. It is recalled that it is computed from the constitutive equation.

From the couples built by the PGD algorithm, we are able to represent explicitly the influence of the orientation of the plies on the transverse displacements for instance. Fig. 15 shows the

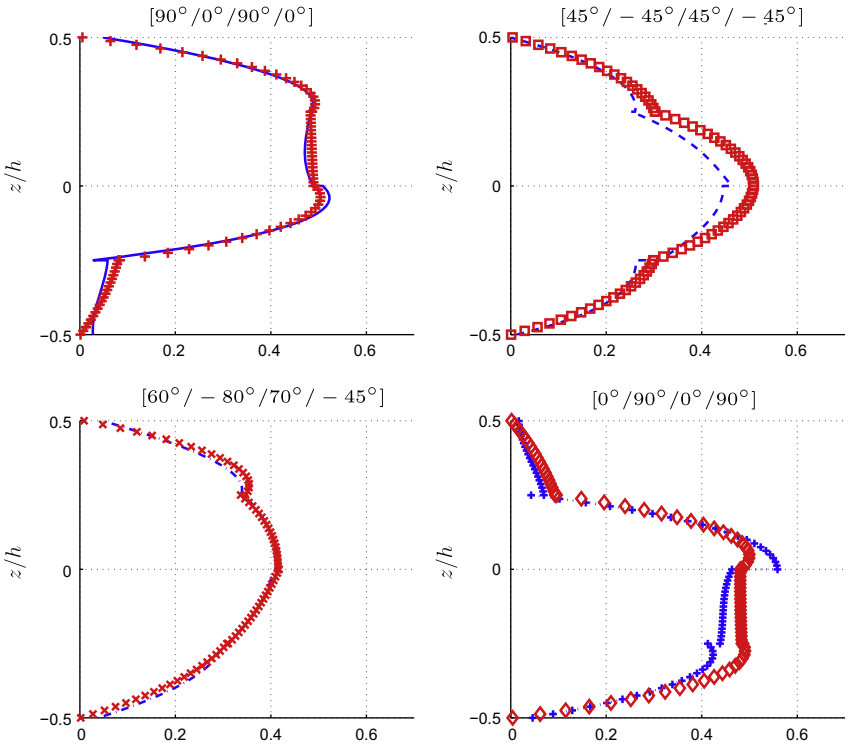

Fig. 14. Distribution of $\bar{\sigma}_{13}$ along the thickness – $S = 4$ – 4 layers – $\theta_i \in [-90, 90]$.

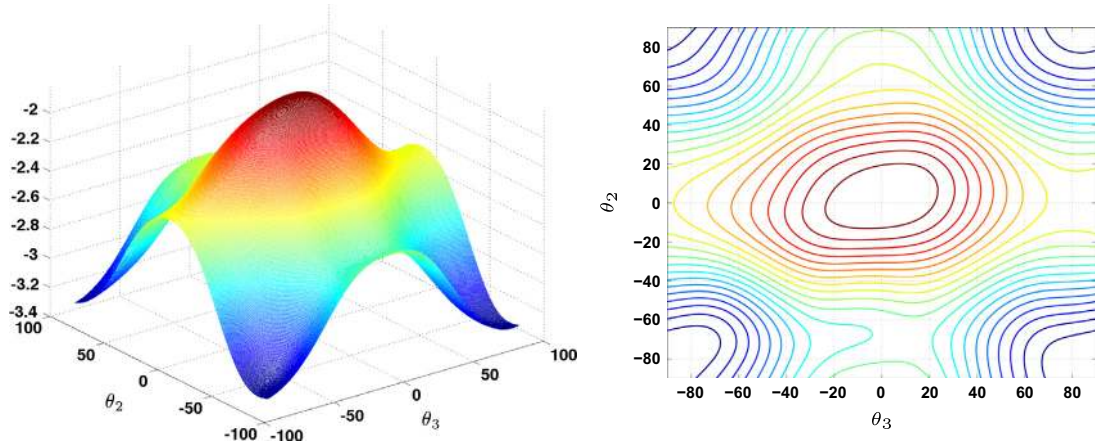

Fig. 15. $w(\theta_2, \theta_3)$ – $S = 4$ – 4 layers – $\theta_1 = 0^\circ,\ \theta_4 = 0^\circ$.

variation of this displacement with respect to θ_2 and θ_3 for a fixed value of θ_1 and θ_4. As expected, the $[0^\circ/0^\circ/0^\circ/0^\circ]$ structure is the stiffest one.

5. Conclusion

In this work, the PGD is applied to derive an explicit solution for the modeling of composite plate structures with any stacking sequences. Indeed, the displacements are expressed as functions of separated variables which involves NC functions depending on the orientation of each ply, and two functions depending on the space coordinates. The construction of these functions is based on greedy type algorithm.

The approach is assessed on various configurations and the results are rather accurate. Moreover, the solution allows us to study directly the influence of the stacking sequences without any additional computational cost, because it does not require the computations of many configurations with fixed laminae orientations. So, the approach can be advantageously used for parametric problems such as optimization, inverse problems and reliability. In fact, these problems require numerous evaluations of the solution as in Monte-Carlo approach. Moreover, the sensitivity of the solution with respect to the angle parameters can be calculated explicitly using the present approach. The added computational cost is negligible. It is the subject of future investigations.

Appendix A. Finite element problem to be solved on Ω

The functions which are assumed to be known, are denoted $\tilde{\mathbf{g}}$ and $\tilde{\mathbf{f}}$ while the function to be computed is denoted $\mathbf{v}$. The strain from Eq. (12) is defined in matrix notations as

$$\boldsymbol{\varepsilon}(\tilde{\mathbf{f}} \circ \mathbf{v}) = \boldsymbol{\Sigma}_z(\tilde{\mathbf{f}})\boldsymbol{\mathcal{E}}_v \tag{A.1}$$

with

$$\boldsymbol{\Sigma}_z(\tilde{\mathbf{f}}) = \begin{bmatrix} 0 & \tilde{f}_1 & 0 & 0 & 0 & 0 & 0 & 0 & 0 \\ 0 & 0 & 0 & 0 & 0 & \tilde{f}_2 & 0 & 0 & 0 \\ 0 & 0 & 0 & 0 & 0 & 0 & \tilde{f}'_3 & 0 & 0 \\ 0 & 0 & 0 & \tilde{f}'_2 & 0 & 0 & 0 & 0 & \tilde{f}_3 \\ \tilde{f}'_1 & 0 & 0 & 0 & 0 & 0 & 0 & \tilde{f}_3 & 0 \\ 0 & 0 & \tilde{f}_1 & 0 & \tilde{f}_2 & 0 & 0 & 0 & 0 \end{bmatrix} \tag{A.2}$$

$$\boldsymbol{\mathcal{E}}_v^T = [\, v_1 \quad v_{1,1} \quad v_{1,2} \quad v_2 \quad v_{2,1} \quad v_{2,2} \quad v_3 \quad v_{3,1} \quad v_{3,2} \,]$$

The variational problem defined on Ω from Eq. (19) is

$$\int_\Omega \boldsymbol{\mathcal{E}}_v^{*T} \mathbf{k}_{\theta z}(\tilde{\mathbf{g}}, \tilde{\mathbf{f}}) \boldsymbol{\mathcal{E}}_v d\Omega = \int_\Omega \mathbf{v}^{*T} \mathbf{t}_{\theta z}(\tilde{\mathbf{g}}, \tilde{\mathbf{f}}) d\Omega - \int_\Omega \boldsymbol{\mathcal{E}}_v^{*T} \boldsymbol{\sigma}_{\theta z}(\tilde{\mathbf{g}}, \tilde{\mathbf{f}}, \mathbf{u}^n) d\Omega \tag{A.3}$$

with

$$\mathbf{k}_{\theta z}(\tilde{\mathbf{g}}, \tilde{\mathbf{f}}) = \int_{\Omega_z \times \mathcal{I}_1 \times \mathcal{I}_2 \ldots \times \mathcal{I}_{NC}} \left[\boldsymbol{\Sigma}_z(\tilde{\mathbf{f}})^T \mathbf{C} \boldsymbol{\Sigma}_z(\tilde{\mathbf{f}}) \prod_{j=1}^{NC} \tilde{g}_j^2 \right] dz d\theta_1 \ldots d\theta_{NC} \tag{A.4}$$

$$\mathbf{t}_{\theta z}(\tilde{\mathbf{g}}, \tilde{\mathbf{f}}) = \int_{\mathcal{I}_1 \times \mathcal{I}_2 \ldots \times \mathcal{I}_{NC}} \left[\tilde{\mathbf{f}} \circ \mathbf{t}\, \pi(\tilde{\mathbf{g}}) \right] d\theta_1 \ldots d\theta_{NC} \Big|_{z=z_F} \tag{A.5}$$

$$\boldsymbol{\sigma}_{\theta z}(\tilde{\mathbf{g}}, \tilde{\mathbf{f}}, \mathbf{u}^n) = \int_{\Omega_z \times \mathcal{I}_1 \times \mathcal{I}_2 \ldots \times \mathcal{I}_{NC}} \left[\boldsymbol{\Sigma}_z(\tilde{\mathbf{f}})^T \mathbf{C} \boldsymbol{\varepsilon}(\mathbf{u}^n)\, \pi(\tilde{\mathbf{g}}) \right] dz d\theta_1 \ldots d\theta_{NC} \tag{A.6}$$

The introduction of the finite element approximation Eq. (20) in the variational Eq. (A.3) leads to the linear system

$$\mathbf{K}_{\theta z}(\tilde{\mathbf{g}}, \tilde{\mathbf{f}}) \mathbf{q}^v = \boldsymbol{\mathcal{R}}_v(\tilde{\mathbf{g}}, \tilde{\mathbf{f}}, \mathbf{u}^n) \tag{A.7}$$

where

- $\mathbf{q}^v$ is the vector of the nodal displacements associated with the finite element mesh in Ω,
- $\mathbf{K}_{\theta z}(\tilde{\mathbf{g}}, \tilde{\mathbf{f}})$ is the stiffness matrix obtained by summing the elements' stiffness matrices $\mathbf{K}^e_{\theta z}(\tilde{\mathbf{g}}, \tilde{\mathbf{f}}) = \int_{\Omega_e} \mathbf{B}_{xy}^T \mathbf{k}_{\theta z}(\tilde{\mathbf{g}}, \tilde{\mathbf{f}}) \mathbf{B}_{xy} d\Omega_e$
- $\boldsymbol{\mathcal{R}}_v(\tilde{\mathbf{g}}, \tilde{\mathbf{f}}, \mathbf{u}^n)$ is the equilibrium residual obtained by summing the elements' residual load vectors $\boldsymbol{\mathcal{R}}^e_v(\tilde{\mathbf{g}}, \tilde{\mathbf{f}}, \mathbf{u}^n) = \int_{\Omega_e} \mathbf{N}_{xy}^T \mathbf{t}_{\theta z}(\tilde{\mathbf{g}}, \tilde{\mathbf{f}}) d\Omega_e - \int_{\Omega_e} \mathbf{B}_{xy}^T \boldsymbol{\sigma}_{\theta z}(\tilde{\mathbf{g}}, \tilde{\mathbf{f}}, \mathbf{u}^n) d\Omega_e$

Appendix B. Finite element problem to be solved on $_z$

In this section, the functions which are assumed to be known, are denoted $\tilde{\mathbf{g}}$ and $\tilde{\mathbf{v}}$ while the function to be computed is denoted $\mathbf{f}$. The strain from Eq. (12) is defined in matrix notations as

$$\boldsymbol{\varepsilon}(\tilde{\mathbf{v}} \circ \mathbf{f}) = \boldsymbol{\Sigma}_{xy}(\tilde{\mathbf{v}}) \boldsymbol{\mathcal{E}}_f \tag{B.1}$$

with

$$\boldsymbol{\Sigma}_{xy}(\tilde{\mathbf{v}}) = \begin{bmatrix} \tilde{v}_{1,1} & 0 & 0 & 0 & 0 & 0 \\ 0 & 0 & \tilde{v}_{2,2} & 0 & 0 & 0 \\ 0 & 0 & 0 & 0 & 0 & \tilde{v}_3 \\ 0 & 0 & 0 & \tilde{v}_2 & \tilde{v}_{3,2} & 0 \\ 0 & \tilde{v}_1 & 0 & 0 & \tilde{v}_{3,1} & 0 \\ \tilde{v}_{1,2} & 0 & \tilde{v}_{2,1} & 0 & 0 & 0 \end{bmatrix} \text{ and } \boldsymbol{\mathcal{E}}_f = \begin{bmatrix} f_1 \\ f'_1 \\ f_2 \\ f'_2 \\ f_3 \\ f'_3 \end{bmatrix} \tag{B.2}$$

The variational problem defined on Ω_z from Eq. (18) is

$$\int_{\Omega_z} \boldsymbol{\mathcal{E}}_f^{*T} \mathbf{k}_{\theta xy}(\tilde{\mathbf{g}}, \tilde{\mathbf{v}}) \boldsymbol{\mathcal{E}}_f dz = \mathbf{f}^{*T} \mathbf{t}_{\theta xy}(\tilde{\mathbf{g}}, \tilde{\mathbf{v}})\Big|_{z=z_F} - \int_{\Omega_z} \boldsymbol{\mathcal{E}}_f^{*T} \boldsymbol{\sigma}_{xy}(\tilde{\mathbf{g}}, \tilde{\mathbf{v}}, \mathbf{u}^n) dz \tag{B.3}$$

with

$$\mathbf{k}_{\theta xy}(\tilde{\mathbf{g}}, \tilde{\mathbf{v}}) = \int_{\Omega \times \mathcal{I}_1 \times \mathcal{I}_2 \ldots \times \mathcal{I}_{NC}} \left[\boldsymbol{\Sigma}_{xy}(\tilde{\nu})^T \mathbf{C} \boldsymbol{\Sigma}_{xy}(\tilde{\nu}) \prod_{j=1}^{NC} \tilde{g}_j^2 \right] d\theta_1 \ldots d\theta_{NC}\, d\Omega \tag{B.4}$$

$$\mathbf{t}_{\theta xy}(\tilde{\mathbf{g}}, \tilde{\mathbf{v}}) = \int_{\Omega \times \mathcal{I}_1 \times \mathcal{I}_2 \ldots \times \mathcal{I}_{NC}} [\tilde{\mathbf{v}} \circ \mathbf{t}\, \pi(\tilde{\mathbf{g}})]\, d\theta_1 \ldots d\theta_{NC}\, d\Omega \tag{B.5}$$

$$\boldsymbol{\sigma}_{xy}(\tilde{\mathbf{g}}, \tilde{\mathbf{v}}, \mathbf{u}^n) = \int_{\Omega \times \mathcal{I}_1 \times \mathcal{I}_2 \ldots \times \mathcal{I}_{NC}} \left[\boldsymbol{\Sigma}_{xy}(\tilde{\mathbf{v}})^T \mathbf{C} \boldsymbol{\varepsilon}(\mathbf{u}^n)\, \pi(\tilde{\mathbf{g}}) \right] d\theta_1 \ldots d\theta_{NC}\, d\Omega \tag{B.6}$$

The introduction of the finite element discretization Eq. (20) in the variational Eq. (B.3) leads to the linear system

$$\mathbf{K}_{\theta xy}(\tilde{\mathbf{g}}, \tilde{\mathbf{v}})\, \mathbf{q}^f = \mathcal{R}_f(\tilde{\mathbf{g}}, \tilde{\mathbf{v}}, \mathbf{u}^n) \tag{B.7}$$

where $\mathbf{q}^f$ is the vector of degree of freedom associated with the polynomial expansion in Ω_z, $\mathbf{K}_{\theta xy}(\tilde{\mathbf{g}}, \tilde{\mathbf{v}})$ is a stiffness matrix defined by Eq. (B.8) and $\mathcal{R}_f(\tilde{\mathbf{g}}, \tilde{\mathbf{v}}, \mathbf{u}^n)$ an equilibrium residual defined by Eq. (B.9)

$$\mathbf{K}_{\theta xy}(\tilde{\mathbf{g}}, \tilde{\mathbf{v}}) = \int_{\Omega_z} \mathbf{B}_z^T \mathbf{k}_{\theta xy}(\tilde{\mathbf{g}}, \tilde{\mathbf{v}}) \mathbf{B}_z dz \tag{B.8}$$

$$\mathcal{R}_f(\tilde{\mathbf{g}}, \tilde{\mathbf{v}}, \mathbf{u}^n) = \mathbf{N}_z^T \mathbf{t}_{\theta xy}(\tilde{\mathbf{g}}, \tilde{\mathbf{v}})\Big|_{z=z_F} - \int_{\Omega_z} \mathbf{B}_z^T \boldsymbol{\sigma}_{xy}(\tilde{\mathbf{g}}, \tilde{\mathbf{v}}, \mathbf{u}^n) dz \tag{B.9}$$

References

[1] Tanigawa Y, Murakami H, Ootao Y. Transient thermal stress analysis of a laminated composite beam. J Therm Stress 1989;12:25–39.
[2] Yang P, Norris C, Stavsky Y. Elastic wave propagation in heterogeneous plates. Int J Solids Struct 1966;2:665–84.
[3] Cook G, Tessler A. A {3,2}-order bending theory for laminated composite and sandwich beams. Compos Part B: Eng J 1998;29B:565–76.
[4] Kant T, Swaminathan K. Analytical solutions for the static analysis of laminated composite and sandwich plates based on a higher order refined theory. Compos Struct 2002;56:329–44.
[5] Librescu L. On the theory of anisotropic elastic shells and plates. Int J Solids Struct 1967;3:53–68.
[6] Lo K, Christensen R, Wu F. A higher-order theory of plate deformation. Part ii: Laminated plates. J Appl Mech ASME 1977;44:669–76.
[7] Matsunaga H. Assessment of a global higher-order deformation theory for laminated composite and sandwich plates. Compos Struct 2002;56:279–91.
[8] Reddy J. A simple higher-order theory for laminated composite plates. J Appl Mech ASME 1984;51(4):745–52.
[9] Whitney J, Sun C. A higher order theory for extensional motion of laminated composites. J Sound Vibr 1973;30:85–97.
[10] Polit O, Vidal P, D'Ottavio M. Robust c^0 high-order plate finite element for thin to very thick structures: mechanical and thermo-mechanical analysis. Int J Numer Methods Eng 2012;40:429–51. http://dx.doi.org/10.1002/nme.3328.
[11] Carrera E. A priori vs. a posteriori evaluation of transverse stresses in multilayered orthotropic plates. Compos Struct 2000;48(4):245–60.
[12] Kim J-S, Cho M. Enhanced first-order theory based on mixed formulation and transverse normal effect. Int J Solids Struct 2007;44:1256–76.
[13] Ferreira A. Analysis of composite plates using a layerwise shear deformation theory and multiquadrics discretization. Mech Adv Mater Struct 2005;12:99–112.
[14] Icardi U. Higher-order zig-zag model for analysis of thick composite beams with inclusion of transverse normal stress and sublaminates approximations. Compos Part B: Eng J 2001;32:343–54.
[15] Pagano N. Exact solutions for composite laminates in cylindrical bending. J Comp Mater 1969;3:398–411.
[16] Reddy J. On refined computational models of composite laminates. Int J Numer Methods Eng 1989;27:361–82.
[17] Shimpi R, Ainapure A. A beam finite element based on layerwise trigonometric shear deformation theory. Compos Struct 2001;53:153–62.
[18] Carrera E. A study of transverse normal stress effect on vibration of multilayered plates and shells. J Sound Vibr 1999;225:803–29.
[19] Rao M, Desai Y. Analytical solutions for vibrations of laminated and sandwich plates using mixed theory. Compos Struct 2004;63:361–73.
[20] Kapuria S, Dumir P, Ahmed A. An efficient higher order zigzag theory for composite and sandwich beams subjected to thermal loading. Int J Solids Struct 2003;40:6613–31.
[21] Lee C-Y, Liu D, Lu X. Static and vibration analysis of laminated composite beams with an interlaminar shear stress continuity theory. Int J Numer Methods Eng 1992;33:409–24.
[22] Sciuva MD, Icardi U. Numerical assessment of the core deformability effect on the behavior of sandwich beams. Compos Struct 2001;52:41–53.
[23] Ambartsumyan S. Theory of anisotropic plates. Translated from russian by T. Cheron and edited by J.E. Ashton. Technomic Publishing Co; 1969.
[24] Whitney J. The effect of transverse shear deformation in the bending of laminated plates. J Comp Mater 1969;3:534–47.
[25] Vidal P, Polit O. A family of sinus finite elements for the analysis of rectangular laminated beams. Compos Struct 2008;84:56–72. http://dx.doi.org/10.1016/j.compstruct.2007.06.009.
[26] Vidal P, Polit O. A sine finite element using a zig-zag function for the analysis of laminated composite beams. Compos Part B: Eng J 2011;42(6):1671–82. http://dx.doi.org/10.1016/j.compositesb.2011.03.012.
[27] Vidal P, Polit O. A refined sinus plate finite element for laminated and sandwich structures under mechanical and thermomechanical loads. Comput Methods Appl Mech Eng 2013;253:396–412.
[28] Carrera E. Theories and finite elements for multilayered, anisotropic, composite plates and shells. Arch Comput Methods Eng 2002;9:87–140.
[29] Carrera E. Historical review of zig-zag theories for multilayered plates and shells. Appl Mech Rev 2003;56(3):287–308.
[30] Noor A, Burton W. Assessment of computational models for multilayered composite shells. Appl Mech Rev 1990;43(4):67–97.
[31] Reddy J. Mechanics of laminated composite plates – theory and analysis. Boca Raton, FL: CRC Press; 1997.
[32] Zhang Y, Yang C. Recent developments in finite elements analysis for laminated composite plates. Compos Struct 2009;88:147–57.
[33] Ammar A, Mokdada B, Chinesta F, Keunings R. A new family of solvers for some classes of multidimensional partial differential equations encountered in kinetic theory modeling of complex fluids. J Non-Newton Fluid Mech 2006;139:153–76.
[34] Ladevèze P. Nonlinear computational structural mechanics – new approaches and non-incremental methods of calculation. Springer-Verlag; 1999.
[35] Allix O, Vidal P. A new multi-solution approach suitable for structural identification problems. Comput Methods Appl Mech Eng 2002;191(25–26):2727–58.
[36] Vidal P, Gallimard L, Polit O. Composite beam finite element based on the proper generalized decomposition. Comput Struct 2012;102–103:76–86. http://dx.doi.org/10.1016/j.compstruc.2012.03.008.
[37] Bognet B, Bordeu F, Chinesta F, Leygue A, Poitou A. Advanced simulation of models defined in plate geometries: 3d solutions with 2d computational complexity. Comput Methods Appl Mech Eng 2012;201–204:1–12. http://dx.doi.org/10.1016/j.cma.2011.08.025.
[38] Vidal P, Gallimard L, Polit O. Proper generalized decomposition and layer-wise approach for the modeling of composite plate structures. Int J Solids Struct 2013;50(14–15):2239–50. http://dx.doi.org/10.1016/j.ijsolstr.2013.03.034.
[39] Savoia M, Reddy J. A variational approach to three-dimensional elasticity solutions of laminated composite plates. J Appl Mech ASME 1992;59:166–75.
[40] Jones RM. Mechanics of composite materials. 2nd ed. Philadelphia, PA: Taylor and Francis; 1999.
[41] Nouy A. A priori model reduction through proper generalized decomposition for solving time-dependent partial differential equations. Comput Methods Appl Mech Eng 2010;199(23–24):1603–26.